Editors' Suggestion

Magnus Hall Effect

Michał Papaj and Liang Fu
Department of Physics, Massachusetts Institute of Technology, Cambridge, Massachusetts 02139, USA

(Received 6 April 2019; revised manuscript received 27 September 2019; published 22 November 2019)

A new type of a linear response Hall effect is predicted in time-reversal-invariant systems with a built-in electric field at zero magnetic field. The Hall response results from a quantum Magnus effect where a self-rotating Bloch electron wave packet moving under an electric field develops an anomalous velocity in the transverse direction. We show that in the ballistic limit the Magnus Hall conductance measures the distribution of the Berry curvature on the Fermi surface.

DOI: 10.1103/PhysRevLett.123.216802

Introduction.—Studies of various Hall effects led to significant progress throughout the history of solid state physics. Starting with the classical Hall effect [1], the anomalous Hall effect [2], the spin Hall effect [3], the thermal Hall effect [4,5], the quantum Hall effect [6], the quantum spin Hall effect [7], and the quantum anomalous Hall effect [8–10] have been discovered. Among these, the classical and anomalous Hall effects appear in time-reversal-breaking systems, where an applied electric field induces a transverse charge current.

An intrinsic contribution to the anomalous Hall effect is associated with the Berry curvature, a fundamental ingredient of modern band theory derived from the electron's wave function [11]. When a Bloch electron is accelerated under an electric field, its electron density distribution within the unit cell changes, which gives rise to an anomalous velocity proportional to the Berry curvature. In time-reversal-breaking systems, the total Berry curvature of the occupied states can be nonzero, resulting in an intrinsic anomalous Hall effect. The impact of the Berry curvature on the transport phenomena has attracted tremendous interest [12–17].

On the other hand, there exists a large class of time-reversal-invariant, inversion-breaking materials which feature a large Berry curvature $\boldsymbol{\Omega}(\boldsymbol{k})$ in momentum space, especially near the gap edge or the band crossing points. Examples include two-dimensional transition metal dichalcogenides (TMDs) [18], graphene multilayer [19,20] and heterostructures [21], topological insulator surface states [22], and Weyl semimetals [23–25]. Because of time-reversal symmetry, the distribution of the Berry curvature satisfies $\boldsymbol{\Omega}(\boldsymbol{k}) = -\boldsymbol{\Omega}(-\boldsymbol{k})$. It is an intriguing question whether such a distribution of the Berry curvature with a zero total can lead to any interesting phenomena in charge transport.

In this work, we demonstrate a new type of linear-response Hall effect induced by the Berry curvature and the built-in electric field in mesoscopic systems under the time-reversal-symmetric condition. We consider electron transport in a Hall bar device made of a 2D material, such as bilayer graphene or a transition metal dichalcogenide. In our setup, the source and drain regions have different carrier densities, which can be achieved by local bottom gates. The difference in the electrostatic potential energy due to the bottom gates $U_s - U_d \equiv \Delta U$ is accompanied by a built-in electric field in the junction in the stationary state, as shown in Fig. 1(a). We study the electrical current in linear response to the applied bias voltage V_{sd}. Since electrons moving from the source to the drain have nonzero net velocity, their wave packets can carry orbital angular momentum and nonzero net Berry curvature. The motion of

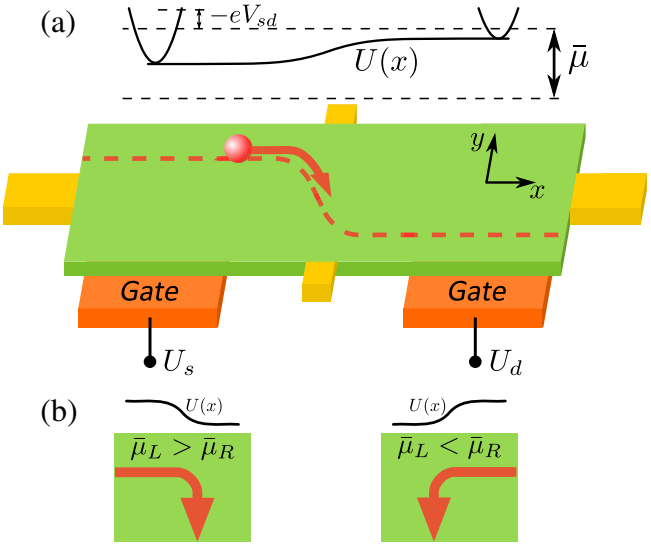

FIG. 1. (a) Geometry of the device for the Magnus Hall effect. Source and drain regions are separated by a segment with a built-in electric field. An electron that exits the source exhibits a Magnus shift Δy_A. Potential energy $U(x)$ profile in the central region determines the position of the band bottom. (b) The direction of the Hall current is preserved under inversion of both the direction of the potential drop and the electrochemical potential bias.

 © 2019 American Physical Society

the chiral Bloch electrons under the built-in electric field leads to a quantum analog of the Magnus effect: as an electron traverses the junction, its center of wave packet acquires a transverse shift. This in turn gives rise to a transverse current linearly proportional to the bias voltage, i.e., a Hall effect. We term this phenomenon the "Magnus Hall effect." It occurs in nonmagnetic systems at zero magnetic field, but relies on the built-in electric field. We show that in the ballistic limit, the Hall conductance is directly related to the Berry curvature distribution of the underlying material.

The Magnus Hall effect is intimately related to the nonlinear Hall effect. This recently theoretically predicted phenomenon occurs in time-reversal-invariant materials in which the dipole moment of Berry curvature, i.e., the Berry curvature dipole, can induce a Hall effect, where the transverse current depends quadratically on the applied electric field [26]. This phenomenon has been subsequently observed in bilayer WTe_2 [27,28]. In the case of the nonlinear Hall effect, reversing the electric field does not change the transverse current. In the Magnus Hall effect, the transverse current is preserved under reversing both the source-drain voltage and the direction of the built-in electric field as presented in Fig. 1(b). In an alternative scenario where the electric field arises from the source-drain voltage V_{sd} itself instead of the bottom gates, the transverse current becomes second order in V_{sd}, resulting in the nonlinear Hall effect. Our work thus opens a pathway to "Hall diodes" for high-frequency nonlinear transport based on the quantum materials that have a significant distribution of Berry curvature.

Electronic Magnus effect.—First we shall consider an electron wave packet that travels inside a sample. The sample has a short segment (between $x = 0$ and $x = L$) within which there is spatially varying potential energy $U(x)$ arising from different gate voltages on the opposite sides [this corresponds to the built-in electric field $\mathbf{E} = (1/e)(\partial U/\partial x)\hat{x} = E_x(x)\hat{x}$]. We assume that $U(x)$ is slowly varying (small built-in electric field) so that wave packets still have well-defined momentum $\mathbf{k}$. This means that the length of the device should be larger than few tens of nanometers. Inside this region, motion of the wave packet is described by the semiclassical equations of motion [12]

$$\dot{\mathbf{r}} = \frac{1}{\hbar}\frac{\partial \epsilon_{\mathbf{k}}}{\partial \mathbf{k}} - \frac{1}{\hbar}\mathbf{\Omega} \times \frac{\partial U}{\partial \mathbf{r}}, \qquad \dot{\mathbf{k}} = -\frac{1}{\hbar}\frac{\partial U}{\partial \mathbf{r}}. \tag{1}$$

Since the built-in electric field is small, wave packet momentum $\mathbf{k}$ does not change substantially under acceleration and remains approximately constant at its initial value $\mathbf{k}_0$. Therefore, the transit time through the electric field region of an incident electron with velocity (v_x, v_y) is simply $t = L/v_x$. During this time, the electron with $v_y \neq 0$ will also travel in the y direction. Importantly, between $x = 0$ and $x = L$ there will be an additional displacement of the wave packet along y due to the anomalous velocity as for 2D systems Berry curvature has only the z component $\mathbf{\Omega}(\mathbf{k}) = \Omega_z(\mathbf{k})\hat{z}$. This displacement is given by

$$\Delta y_A = -\int_0^t \frac{\Omega_z(\mathbf{k})}{\hbar}\frac{\partial U}{\partial x}dt' \approx -\frac{1}{\hbar v_x}\Omega_z(\mathbf{k}_0)\int_0^L \frac{\partial U}{\partial x}dx = \frac{1}{\hbar v_x}\Omega_z(\mathbf{k}_0)\Delta U, \tag{2}$$

with $\Delta U = -\int_0^L (\partial U/\partial x)dx$ being the difference in the potential energy. Therefore, an electron wave packet with a nonzero Berry curvature moving through the region of electric field will acquire an additional shift in the direction perpendicular to the electric field as schematically shown in Fig. 1(a). This in turn leads to a current density in the y direction by integrating single wave packet contribution $-e\Delta y_A/t = -e/(\hbar L)\Omega(\mathbf{k}_0)\Delta U$ over the occupied states. This transverse current vanishes in equilibrium. However, in the current carrying steady state, the modes with positive and negative velocity are not equally occupied. Since in systems with time-reversal symmetry Berry curvature is opposite for $\mathbf{k}$ and $-\mathbf{k}$ states (which also have opposite velocities), this effect can lead to a Hall current even in nonmagnetic materials. To see more clearly how the Hall current arises here, we employ the Boltzmann transport equation.

Boltzmann transport equation solution.—To describe the mesoscopic electron transport in a 2D system we use a collisionless Boltzmann equation (BE),

$$\frac{\partial f}{\partial t} + \dot{\mathbf{r}} \cdot \frac{\partial f}{\partial \mathbf{r}} + \dot{\mathbf{k}} \cdot \frac{\partial f}{\partial \mathbf{k}} = 0, \tag{3}$$

where $f(\mathbf{k}, \mathbf{r})$ is the occupation distribution function. We are looking for a stationary state distribution, so $\partial f/\partial t = 0$. We solve the Boltzmann equation in a geometry of a stripe of infinite width in the y direction and finite length L in the x direction. At $x < 0$ and $x > L$ we have a source and a drain. Since the system is translationally invariant in the y direction, the stationary distribution function will be independent of y.

The wave packets evolve according to the semiclassical equations (1). The energy of the electrons in the segment is

$$\epsilon(\mathbf{k}, \mathbf{r}) = \epsilon_{\mathbf{k}} + U(x), \tag{4}$$

where $\epsilon_{\mathbf{k}}$ is the band energy. In equilibrium, the solution is given by the Fermi-Dirac distribution with constant electrochemical potential $\bar{\mu}$, but with spatially changing energy (4) and can be expressed as

$$f_0(\mathbf{k}, \mathbf{r}) = (e^{\beta[\epsilon(\mathbf{k},\mathbf{r}) - \bar{\mu}]} + 1)^{-1}; \tag{5}$$

$f_0(\mathbf{k}, \mathbf{r})$ is a solution of Boltzmann equation (3) as can be verified using Eq. (1). This solution guarantees that no

current is flowing in the system as at each energy and position the number of states with $\mathbf{k}$ and $-\mathbf{k}$ is equal.

To obtain a solution that corresponds to a steady current flow, we apply a small bias V_{sd} in a form of imbalance of electrochemical potentials between the source and the drain, so that $\bar{\mu}_D = \bar{\mu}$ and $\bar{\mu}_S = \bar{\mu} - eV_{sd} = \bar{\mu} + \Delta\bar{\mu}$. We have to solve BE with boundary conditions that take into account the presence of source and drain at $x = 0$ and $x = L$. Taking into consideration the device geometry of our system, we now look for a solution in the lowest order of the perturbation in the electrochemical potential imbalance. To achieve this, we write $f = f_0 + f_1$, where f_1 is the nonequilibrium part first order in the perturbation $\Delta\bar{\mu}$. This gives an equation for f_1:

$$\frac{1}{\hbar}\frac{\partial f_1}{\partial x}\frac{\partial \epsilon_k}{\partial k_x} - \frac{1}{\hbar}\frac{\partial U}{\partial x}\frac{\partial f_1}{\partial k_x} = 0. \tag{6}$$

Since we assumed that $U(x)$ is slowly varying, the second term on the left-hand side is small, so we drop it and we arrive at $\partial f_1/\partial x = 0$. Therefore, $f_1(\mathbf{k}, \mathbf{r})$ only depends on $\mathbf{k}$. We can now determine its form from the boundary condition. The larger electrochemical potential of the source region results in a surplus of electrons entering the system at the $x = 0$ interface with positive v_x velocity and propagating across the device without any scattering in the ballistic limit. This boundary condition gives us

$$f_1(\mathbf{k}, \mathbf{r}) = \begin{cases} \left(-\frac{\partial f_0}{\partial \epsilon_k}\right)\Delta\bar{\mu} & v_x(\mathbf{k}) > 0 \\ 0 & v_x(\mathbf{k}) < 0, \end{cases} \tag{7}$$

where $v_x(\mathbf{k}) = (1/\hbar)(\partial\epsilon_k/\partial k_x)$. Equipped with this solution, we are able to calculate the longitudinal and the Hall response of our system. We have then

$$j_x = -e\int \frac{d^2k}{(2\pi)^2} v_x f_1 = -\frac{e}{h}\frac{\Delta\bar{\mu}}{2\pi}\int_{v_x(\mathbf{k})>0} d^2k \frac{\partial\epsilon_k}{\partial k_x}\left(-\frac{\partial f_0}{\partial \epsilon_k}\right), \tag{8}$$

$$j_y = -e\int \frac{d^2k}{(2\pi)^2} v_y f_1 = j_y^0 + j_H,$$
$$j_y^0 = -\frac{e}{h}\frac{\Delta\bar{\mu}}{2\pi}\int_{v_x(\mathbf{k})>0} d^2k \frac{\partial\epsilon_k}{\partial k_y}\left(-\frac{\partial f_0}{\partial \epsilon_k}\right), \tag{9}$$

$$j_H = \frac{e}{h}\frac{\Delta\bar{\mu}}{2\pi}\int_{v_x(\mathbf{k})>0} d^2k\, \Omega_z(\mathbf{k})\frac{\partial U}{\partial x}\left(-\frac{\partial f_0}{\partial \epsilon_k}\right). \tag{10}$$

Here the j_y^0 term arises from the Fermi surface anisotropy and depends on its orientation relative to the direction of applied bias $\hat{x}$. Note that j_y^0 is independent of ΔU, which can be used to distinguish it from the Magnus Hall component j_H. However, as we shall show later, the j_y^0 term can also vanish due to symmetry.

To obtain the Hall current due to the Berry curvature, we integrate the anomalous velocity contribution over the whole length of the device $I_y = \int_0^L dx j_H$ and then we can define Hall conductance as $G_H = -eI_y/\Delta\bar{\mu}$ and obtain at $T = 0$,

$$G_H = \frac{e^2}{h}\frac{\Delta U}{2\pi}\int_{v_x(\mathbf{k})>0} d^2k\, \Omega_z(\mathbf{k})\delta(\epsilon_{\mathbf{k}} - \mu), \tag{11}$$

where the electrostatic potential energy difference across the junction $\Delta U = U_s - U_d$ is assumed to be small.

This equation is the main result of this work. First of all, in the limit of small ΔU the Hall response does not depend on the detailed spatial dependence of the potential energy. Second, the dependence on ΔU is linear and the Hall current is independent of the system size in the ballistic limit. The effect is reduced by inclusion of disorder as we show in the Supplemental Material [29].

Crucially, the Magnus Hall current is determined by the Berry curvature of the electrons with a positive velocity along the direction of the applied bias. While the Hall current depends on the integral of the Berry curvature over the Fermi surface, it nevertheless offers two tuning knobs that make it a perfect tool to characterize the Berry curvature distribution. First of all, by applying an overall gate voltage potential, one can tune the chemical potential in the whole device and scan different Fermi surfaces. Second, by varying the direction of the applied bias (rotating the Hall bar geometry) with respect to the crystalline axis, the angular distribution of Berry curvature within a given Fermi surface can be established.

Model.—To demonstrate this effect explicitly, we turn to a concrete model, which breaks inversion symmetry, but preserves time-reversal symmetry. We have chosen a simple two band model with the Hamiltonian

$$H(\mathbf{k}) = Ak^2 + (Bk^2 + \delta)\sigma_z + v_y k_y \sigma_y + D\sigma_x. \tag{12}$$

It contains two massive Dirac cones which are tilted when $A \neq 0$. This model captures the essential features of the tilted Dirac cones of topological crystalline insulator surface states [26] and low-energy band structure of 2D WTe_2 [18]. More details of the model are presented in the Supplemental Material [29].

We can now compute the Berry curvature $\mathbf{\Omega}(\mathbf{k})$ distribution in the Brillouin zone for parameters $A = 0$, $B = 1$, $\delta = -0.25$, $v_y = 1.0$, $D = 0.1$, which is shown in the inset of Fig. 2 for the valence band. While the total Berry curvature integrated over the Brillouin zone is equal to 0, the distribution consists of two peaks of opposite signs, located at the Dirac points.

Furthermore, this model possesses mirror symmetry M_x: $H(k_x, k_y) \to H(-k_x, k_y)$, which guarantees that $\epsilon(k_x, k_y) = \epsilon(-k_x, k_y)$. For $D = 0$, this model has an additional mirror symmetry M_y: $H(k_x, k_y) = \sigma_z H(k_x, -k_y)\sigma_z$.

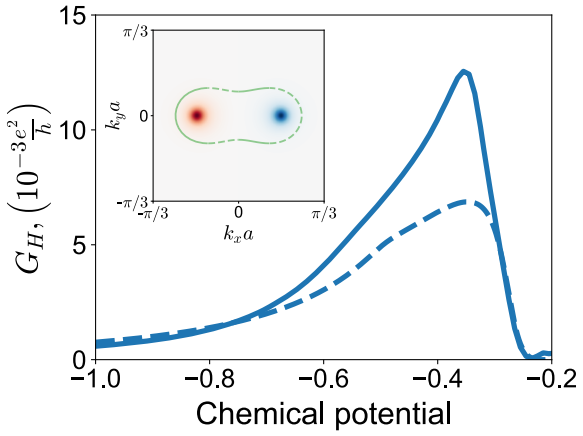

FIG. 2. Magnus Hall conductance G_H as a function of the chemical potential μ at $T = 0.01$ and $\Delta U = 0.05$ from Eq. (11) (dashed) and Landauer-Buttiker simulation (solid). The inset shows the distribution of Berry curvature of the valence bands in the Brillouin zone. The green line shows the Fermi surface for $E = -0.35$ (solid for $v_x > 0$ and dashed for $v_x < 0$).

This symmetry is broken for $D \neq 0$. However, because the model is also time-reversal invariant, we have $\epsilon(-k_x, k_y) = \epsilon(k_x, -k_y)$, which causes the current density j_y^0 of Eq. (9) to vanish. Therefore, the Hall current will be determined solely by the Magnus Hall contribution j_H of Eq. (10) and G_H can be calculated according to Eq. (11). Result of such a calculation is presented as the dashed curve in Fig. 2 as a function of the chemical potential. Even though the total integral of $\Omega(\mathbf{k})$ vanishes, because our result for G_H only relies on the Berry curvature of Bloch states with $v_x > 0$, it is nonzero. For the set of parameters used in the calculation, both bands are symmetric with respect to the $E = 0$ line and so the result for the conduction band is a mirror image of the curve for the valence band. We note that the direction of the Hall current is the same for both bands, because while the Berry curvature switches sign to opposite between the two bands, the velocities for given $\mathbf{k}$ also change to opposite and as a result the integration occurs over the regions with the same values of $\Omega(\mathbf{k})$.

These approximate results derived from the semiclassical Boltzmann transport approach can be compared with a numerical tight-binding simulation using the Landauer-Buttiker method. Details of the calculation are in the Supplemental Material [29]. All the numerical simulations have been performed using the Kwant package [30]. We consider the chemical potential dependence of G_H^{LB}, which we present as the solid curve in Fig. 2 for $L = 200$, $W = 2400$ lattice sites and $\Delta U = 0.05$. The curve is obtained by temperature broadening with $T = 0.01$. The qualitative behavior of the semiclassical result is reproduced with an asymmetric peak positioned away from the band bottom. The difference can be attributed to the differences in the geometry of the setups for numerical simulation (finite width leads injecting current into the system) and semiclassical calculation (infinite width of the setup).

Candidate materials.—To observe the Magnus Hall effect under time-reversal symmetry, several conditions must be satisfied. First of all, the underlying material must break the inversion symmetry in order to have a nonzero Berry curvature in the Brillouin zone. Furthermore, Berry curvature of the right and left moving modes must be asymmetric. For example, under time-reversal symmetry massive Dirac fermions have to appear in pairs with an opposite sign of the Berry curvature. If they are isotropic, there will be an equal number of right movers with both signs of $\Omega(\mathbf{k})$ in each Dirac valley and their contributions will cancel each other. However, in general the Dirac cones are not perfectly isotropic and perfect cancellation will not occur. Two examples of materials that satisfy this condition are monolayer graphene on hBN (sublattice symmetry is broken due to formation of the moiré superlattice) [21,31–33] and bilayer graphene with perpendicular electric field applied [19,20,34]. In both cases trigonal warping introduces asymmetry between the right and left movers in each valley. Moreover, these platforms support devices of high quality, which enable ballistic motion of electrons [35–37], beneficial for observation of the predicted effect.

As an example we use a model of bilayer graphene with trigonal warping and perpendicular electric field that opens up a gap. Calculations are performed using a low-energy Hamiltonian that describes both the K and K' valleys of bilayer graphene (labeled by $s = \pm 1$) [34]:

$$H_s = \begin{pmatrix} \Delta & svk_{-s} - \lambda k_s^2 \\ svk_s - \lambda k_{-s}^2 & -\Delta \end{pmatrix}, \qquad (13)$$

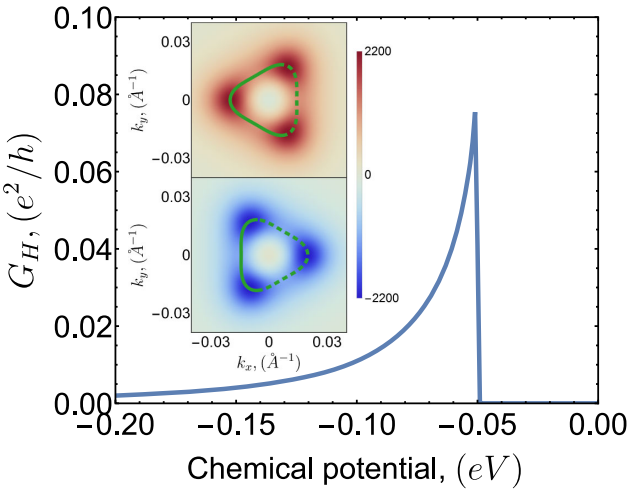

FIG. 3. Hall conductance for the bilayer graphene model for $\Delta U = 10$ meV. Inset: Berry curvature distribution around the K and K' valley of the valence band of bilayer graphene. The green line shows the Fermi surface at $\mu = -60$ meV (solid for $v_x > 0$ and dashed for $v_x < 0$).

where $k_\pm = k_x \pm ik_y$. Berry curvature distribution near both valleys is presented in the inset of Fig. 3. The parameters used in the calculations are $\Delta = 50$ meV, $v = 10^5$ m/s, and $\lambda = 1/(2m^*)$ with effective mass $m^* = 0.033m_e$, m_e being the electron mass [19,38]. The Fermi surface at $\mu = -60$ meV is indicated by the green line, solid for $v_x = (1/\hbar)(\partial\epsilon_k/\partial k_x) > 0$, and dashed for $v_x < 0$. We can now use this to compute the Hall conductance as a function of chemical potential in the vicinity of the band edge using the analytical formula (11), which is shown in Fig. 3 for $\Delta U = 10$ meV and taking spin degeneracy into account. Our result demonstrates explicitly that the Magnus Hall effect does not rely on the Berry curvature dipole [26,39–44] (which is absent in bilayer graphene with trigonal warping) or the presence of skew scattering [45–48] that are necessary conditions for the nonlinear Hall effect.

Summary.—In this Letter we have demonstrated the existence of the Magnus Hall effect in inversion symmetry breaking, but time-reversal-invariant systems that have nonzero Berry curvature. The effect relies on a built-in electric field in the device and should be most pronounced in ballistic systems. Therefore, the device should be shorter than the mean free path, while also being long enough in order to allow for the slow variation of the potential energy. For bilayer graphene this translates to the length of the junction between 100 nm and 1 μm. Since both the bottom gate separation and the applied voltage can be controlled experimentally, we believe that it should be possible to tune the device into the most optimal regime for sufficiently clean samples.

The significance of the Magnus Hall effect is twofold. First, it opens a pathway to a new generation of current rectification devices. Furthermore, it also provides a much needed tool to map Berry curvature distribution of quantum materials in momentum space.

We thank Hiroki Isobe and Su-Yang Xu for helpful discussions. This work was supported by the U.S. Department of Energy (DOE), Office of Basic Energy Sciences under Award No. DE-SC0018945. M. P. was supported by Shell through the MIT Energy Initiative. L. F. was supported in part by a Simons Investigator Award from the Simons Foundation.

[1] E. H. Hall, Am. J. Math. **2**, 287 (1879).
[2] N. Nagaosa, J. Sinova, S. Onoda, A. H. MacDonald, and N. P. Ong, Rev. Mod. Phys. **82**, 1539 (2010).
[3] J. Sinova, S. O. Valenzuela, J. Wunderlich, C. H. Back, and T. Jungwirth, Rev. Mod. Phys. **87**, 1213 (2015).
[4] M. Banerjee, M. Heiblum, V. Umansky, D. E. Feldman, Y. Oreg, and A. Stern, Nature (London) **559**, 205 (2018).
[5] Y. Kasahara, T. Ohnishi, Y. Mizukami, O. Tanaka, S. Ma, K. Sugii, N. Kurita, H. Tanaka, J. Nasu, Y. Motome, T. Shibauchi, and Y. Matsuda, Nature (London) **559**, 227 (2018).
[6] K. v. Klitzing, G. Dorda, and M. Pepper, Phys. Rev. Lett. **45**, 494 (1980).
[7] C. L. Kane and E. J. Mele, Phys. Rev. Lett. **95**, 226801 (2005).
[8] F. D. M. Haldane, Phys. Rev. Lett. **61**, 2015 (1988).
[9] C.-Z. Chang *et al.*, Science **340**, 167 (2013).
[10] C.-X. Liu, S.-C. Zhang, and X.-L. Qi, Annu. Rev. Condens. Matter Phys. **7**, 301 (2016).
[11] R. Karplus and J. M. Luttinger, Phys. Rev. **95**, 1154 (1954).
[12] D. Xiao, M.-C. Chang, and Q. Niu, Rev. Mod. Phys. **82**, 1959 (2010).
[13] J. E. Moore and J. Orenstein, Phys. Rev. Lett. **105**, 026805 (2010).
[14] T. Morimoto, S. Zhong, J. Orenstein, and J. E. Moore, Phys. Rev. B **94**, 245121 (2016).
[15] T. Morimoto and N. Nagaosa, Sci. Adv. **2**, e1501524 (2016).
[16] S. Chaudhary, M. Endres, and G. Refael, Phys. Rev. B **98**, 064310 (2018).
[17] M. S. Rudner and J. C. W. Song, arXiv:1807.01708.
[18] X. Qian, J. Liu, L. Fu, and J. Li, Science **346**, 1344 (2014).
[19] E. McCann and M. Koshino, Rep. Prog. Phys. **76**, 056503 (2013).
[20] A. V. Rozhkov, A. O. Sboychakov, A. L. Rakhmanov, and F. Nori, Phys. Rep. **648**, 1 (2016).
[21] M. Yankowitz, J. Xue, D. Cormode, J. D. Sanchez-Yamagishi, K. Watanabe, T. Taniguchi, P. Jarillo-Herrero, P. Jacquod, and B. J. LeRoy, Nat. Phys. **8**, 382 (2012).
[22] L. Fu, Phys. Rev. Lett. **103**, 266801 (2009).
[23] M. Z. Hasan, S.-Y. Xu, I. Belopolski, and S.-M. Huang, Annu. Rev. Condens. Matter Phys. **8**, 289 (2017).
[24] N. P. Armitage, E. J. Mele, and A. Vishwanath, Rev. Mod. Phys. **90**, 015001 (2018).
[25] B. Yan and C. Felser, Annu. Rev. Condens. Matter Phys. **8**, 337 (2017).
[26] I. Sodemann and L. Fu, Phys. Rev. Lett. **115**, 216806 (2015).
[27] Q. Ma, S.-Y. Xu, H. Shen, D. MacNeill, V. Fatemi, T.-R. Chang, A. M. M. Valdivia, S. Wu, Z. Du, C.-H. Hsu, S. Fang, Q. D. Gibson, K. Watanabe, T. Taniguchi, R. J. Cava, E. Kaxiras, H.-Z. Lu, H. Lin, L. Fu, N. Gedik, and P. Jarillo-Herrero, Nature (London) **565**, 337 (2019).
[28] K. Kang, T. Li, E. Sohn, J. Shan, and K. F. Mak, Nat. Mater. **18**, 324 (2019).
[29] See Supplemental Material at http://link.aps.org/supplemental/10.1103/PhysRevLett.123.216802 for the details of the toy model, the numerical simulations and the results with disorder.
[30] C. W. Groth, M. Wimmer, A. R. Akhmerov, and X. Waintal, New J. Phys. **16**, 063065 (2014).
[31] C.-H. Park, L. Yang, Y.-W. Son, M. L. Cohen, and S. G. Louie, Phys. Rev. Lett. **101**, 126804 (2008).
[32] B. Hunt, J. D. Sanchez-Yamagishi, A. F. Young, M. Yankowitz, B. J. LeRoy, K. Watanabe, T. Taniguchi, P. Moon, M. Koshino, P. Jarillo-Herrero, and R. C. Ashoori, Science **340**, 1427 (2013).
[33] M. Yankowitz, J. Jung, E. Laksono, N. Leconte, B. L. Chittari, K. Watanabe, T. Taniguchi, S. Adam, D. Graf, and C. R. Dean, Nature (London) **557**, 404 (2018).

[34] E. McCann and V. I. Fal'ko, Phys. Rev. Lett. **96**, 086805 (2006).
[35] X. Du, I. Skachko, A. Barker, and E. Y. Andrei, Nat. Nanotechnol. **3**, 491 (2008).
[36] A. S. Mayorov, R. V. Gorbachev, S. V. Morozov, L. Britnell, R. Jalil, L. A. Ponomarenko, P. Blake, K. S. Novoselov, K. Watanabe, T. Taniguchi, and A. K. Geim, Nano Lett. **11**, 2396 (2011).
[37] L. Banszerus, M. Schmitz, S. Engels, M. Goldsche, K. Watanabe, T. Taniguchi, B. Beschoten, and C. Stampfer, Nano Lett. **16**, 1387 (2016).
[38] M. Mucha-Kruczyński, E. McCann, and V. I. Fal'ko, Semicond. Sci. Technol. **25**, 033001 (2010).
[39] J. I. Facio, D. Efremov, K. Koepernik, J.-S. You, I. Sodemann, and J. van den Brink, Phys. Rev. Lett. **121**, 246403 (2018).
[40] S. S. Tsirkin, P. A. Puente, and I. Souza, Phys. Rev. B **97**, 035158 (2018).
[41] J.-S. You, S. Fang, S.-Y. Xu, E. Kaxiras, and T. Low, Phys. Rev. B **98**, 121109(R) (2018).
[42] Y. Zhang, Y. Sun, and B. Yan, Phys. Rev. B **97**, 041101(R) (2018).
[43] Y. Zhang, J. van den Brink, C. Felser, and B. Yan, 2D Mater. **5**, 044001 (2018).
[44] L.-k. Shi and J. C. W. Song, Phys. Rev. B **99**, 035403 (2019).
[45] H. Isobe, S.-Y. Xu, and L. Fu, arXiv:1812.08162.
[46] S. Nandy and I. Sodemann, arXiv:1901.04467.
[47] E. J. König, M. Dzero, A. Levchenko, and D. A. Pesin, Phys. Rev. B **99**, 155404 (2019).
[48] Z. Z. Du, C. M. Wang, S. Li, H.-Z. Lu, and X. C. Xie, Nat. Commun. **10**, 3047 (2019).